ACS APPLIED MATERIALS & INTERFACES

www.acsami.org

Research Article

Ion Motor as a New Universal Strategy for the Boosting the Performance of Zn-Ion Batteries

Lulu Chai, Junqing Pan,* Xiaoyang Zhu, Yanzhi Sun, Xiaoguang Liu, Wei Li, Jinjie Qian, Xifei Li,* and Xueliang Sun*

Cite This: *ACS Appl. Mater. Interfaces* 2022, 14, 30839−30846

Read Online

ACCESS | Metrics & More | Article Recommendations | Supporting Information

ABSTRACT: The quiescent electrolyte causes serious concentration polarization and dendrite problems during the charging and discharging of the battery, which restricts the development of metal secondary batteries and flow batteries. Herein, we report a new concept of ion motors, with which the directional driving and uniformity of the electrolyte are realized to eliminate the concentration polarization and dendritic phenomenon for secondary metal batteries and flow batteries without additional external energy. In this study, a dendrite-free secondary metal battery with ion motors is constructed to eliminate a considerable concentration polarization voltage by a tiny induced counter electromotive force generated by Lorentz force, significantly improving the output power and energy efficiency of the battery. An actual pump-free flow battery with an ion motor is also assembled, which overcomes the problems of low energy efficiency and the complex structure caused by the traditional flow battery requiring 1−2 pumps to drive the electrolyte. The efficiency of ion motors to drive the electrolyte is hundreds of times higher than that of the mechanical pump. Therefore, the ion motor provides a universal strategy for designing more pump-free flow batteries and metal secondary batteries without the risk of dendrites in the future.

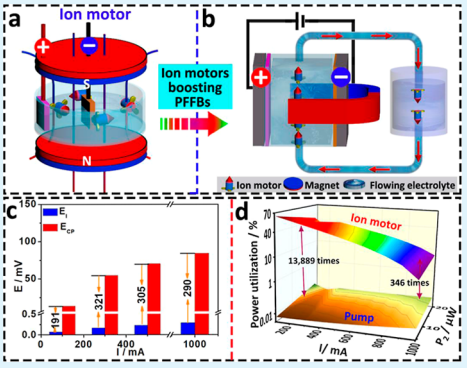

KEYWORDS: *ion motor, pump-free flow battery, electrolyte flow, Zn−Ni prototype battery, dendrite growth*

1. INTRODUCTION

The development of high-performance electrochemical energy storage (EES) systems, such as lithium-/sodium-ion batteries,[1−4] metal secondary batteries,[5−10] and flow batteries,[11−13] can not only achieve highly efficient storage and conversion of renewable energy but also promote the commercialization of electric vehicles, and it significantly reduces the demand for fossil energy and carbon dioxide emissions, thereby accelerating the realization of the global "carbon neutrality" goal.[14−16]

Generally, batteries are composed of anodes, cathodes, and electrolytes, which achieve the charging and discharging process of batteries. The directional flow of the electrolyte is extremely important because it helps in the diffusion process of ions, eliminating the concentration polarization formed on the electrolyte.[17−20] Furthermore, it accelerates the renewal of active materials on the electrode surface and improves the output power and durability of the battery.[21−25] In the gravitational field, the ion concentration gradient generated during the charging and discharging process causes serious concentration polarization and dendrite problems, even causing accidents such as the internal short circuit of the battery,[26−28] which dramatically reduces the energy efficiency and cycle life of batteries. Among the reported batteries, the existing flow batteries must be equipped with pumps to drive the electrolyte flow during the charging and discharging process.[29−32] Furthermore, the existence of mechanical pumps causes the following three problems in the actual application of flow batteries: (1) 1−2 pumps consume 5−10% of energy, which reduce the output energy of the battery. (2) The pump containing the flow battery has a more complex structure, which increases the cost of manufacture and maintenance and reduces the reliability of the flow battery. (3) It is difficult to effectively agitate the electrolyte inside the battery, insufficiently releasing electrolyte polarization. Therefore, there is an urgent requirement to invent a revolutionary universal electrolyte-driving technology to achieve a continuous directional flow of the electrolyte for all the related batteries and electrolysis cells, especially for the modern fully sealed batteries. It is a pity that the relevant research has not been reported so far.

Here, we report a new concept of "ion motor", by which the ions of directional movement construct a microion motor for

Received: April 8, 2022
Accepted: June 17, 2022
Published: June 28, 2022

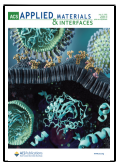

https://doi.org/10.1021/acsami.2c06146
ACS Appl. Mater. Interfaces 2022, 14, 30839−30846

driving electrolytes to move during electrochemical reactions of batteries via Lorentz force (Figure 1a,b). First, this strategy

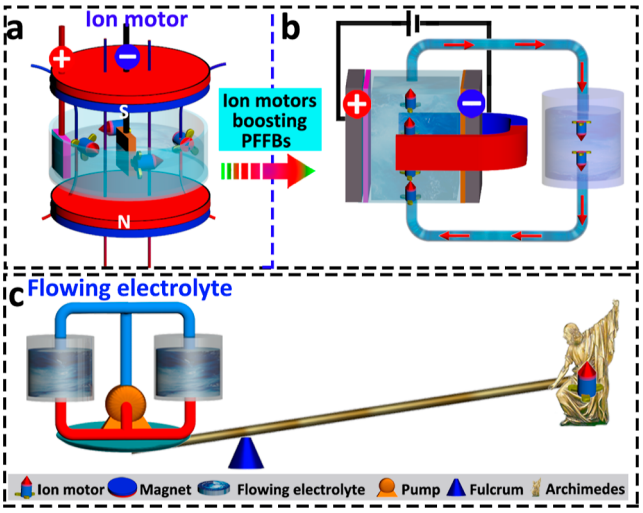

Figure 1. Schematic illustration of the ion motor-driven metal secondary battery and flow battery. (a) Model of the ion motor affected by the magnetic field; (b) model of the ion motor-driven pump-free flow battery; (c) schematic illustration of ion motor-driven electrolyte as a lever fulcrum to push the electrolyte.

is that every ion of the electrolyte contributes to driving the electrolyte. The drive efficiency of the ion motor is hundreds of times that of the mechanical pump, exhibiting an excellent leverage effect (Figure 1c). Then, the tiny induced counter electromotive force of 0.07−0.29 mV at the current of 100−1000 mA driven by the magnetic field can eliminate the concentration polarization of 13.4−84.0 mV, achieving an effect up to hundreds of times, significantly improving the high current capability and energy efficiency of the battery. In addition, the ion motor is a durable, maintenance-free, and contactless electrolyte-driving strategy. The assembled dendrite-free metal secondary battery shows that it is possible to eliminate dendrite problems caused by the ion concentration gradient for fully sealed metal secondary batteries in the future. In the assembled ion motor-driven zinc secondary battery (ZSB), the electrolyte automatically circles around for 3150 laps in a discharge process at 100 mA, far exceeding the requirement of eliminating the concentration gradient (Figure 2a). Besides, a revolutionary pump-free Zn flow battery (ZFB) is also designed by the ion motor strategy. The ion motor can replace the traditional mechanical pump to significantly reduce the structural complexity and manufacturing costs, improving reliability and energy efficiency. Furthermore, the strategy can automatically adjust the driving force by tuning the current, which is impossibly realized for general electric stirrers or pumps. This strategy will be widely accepted for application in various batteries and electrolysis processes, especially for improving the electrochemical performance of lithium-ion batteries in winter.

2. EXPERIMENTAL SECTION

2.1. Dendrite-Free ZSB Test. A ϕ 80 mm × 40 mm weighing bottle was used as the shell for the cylindrical battery. A piece of copper foil (11.0 × 2.5 cm) was rolled into a cylindrical anode on a plastic tube (ϕ 3.5 × 4.0 cm) and set upright at the center of the bottle bottom. A sintered bent NiOOH sheet (11.0 × 2.5 cm) was employed as an arc cathode and placed against the inner wall of the bottle shell. Both electrodes were stuck and sealed with epoxy. The radial distance between the anode and cathode was 1.5 cm. The battery was placed on a round magnet (N52, ϕ 80 mm, Ningbo Magnet Ltd.) with the north pole (N) upward and south pole (S) downward. The magnet had an effective magnetic field strength of around 350 mT. This assembly was called the horizontal Zn secondary battery, meaning that the magnet instead of electrodes was placed horizontally. 80 mL of 6 M KOH and 0.35 M ZnO solution (mass: 100 g) was used as an electrolyte. Galvanostatic charge−discharge (GCD) curves were measured by the LANHE system at different current densities at room temperature. The velocity and number of circulation in each charge−discharge cycle were measured by the following procedure: a microplastic floating ball used as an indicator was floated on the electrolyte. It circled around the battery driven by Lorentz force in the magnetic field. The consumed time in one circle was visually counted, and the velocity and the total circle numbers per cycle were calculated. During GCD tests, the battery was operated at different currents with designated charging capacity and discharge cutoff voltage. For comparison, the batteries without ion motor driving are also tested without a magnet.

2.2. Pump-Free ZFB Test. A cubic vessel made of acrylic [polymethyl methacrylate (PMMA)] plastics (2 × 2 cm^2 in bottom area and 3.5 cm in height) with a cover was used as a battery shell. An anode of copper foil (30 μm in thickness) and a cathode of sintered NiOOH sheet (1.0 mm in thickness) 1.5 cm wide and 2.8 cm high were erected face to face against the opposite two walls with an electrode distance of 1.5 cm. A transparent PMMA electrolyte circulation tube (inner diameter: 1.2 cm) with four elbows and an upper tee was connected to the cover and bottom. The vessel and all the connection joints were sealed air-tight with epoxy. The vessel and the whole circulation tube were filled with the electrolyte, adjusted by a valve connected to the upper tee. Two rectangle magnets each were fixed on the other two opposite external walls, perpendicular to the electrodes, and the magnetic field strength was around 350 mT. This assembly was called a vertical Zn pump-free flow battery, meaning that the magnets were placed vertically. 40 mL of 6 M KOH and 0.35 M ZnO solution (mass: 50 g) was used as an electrolyte. The charge−discharge test was conducted at room temperature. GCD tests were performed at 10, 20, 30, 50, and 70 mA with a charging capacity of 120 mAh and a discharge cutoff voltage of 1.0 V. The batteries without ion motor driving were also tested in the same way for comparison.

2.3. Morphology Characterization. A field emission scanning electron microscopy (FE-SEM) system from Supra 55, ZEISS, Germany, was employed to characterize the morphology of the samples. The SEM images and energy-dispersive X-ray spectroscopy (EDS) spectra were acquired by using a model Supra 55, ZEISS of a FE-SEM system operated at 10 kV.

2.4. Electrolyte Concentration Measurement in Different Areas of the Horizontal ZSB. The analysis method of Zn^{2+} concentration in the electrolyte is as follows: after charging and discharging the battery for six cycles at different currents, a microsyringe was used to separately suck 1.00 mL of electrolyte from four different areas along the vertical direction close to the anode surface, which were nominated as areas A, B, C, and D.

The detection of Zn^{2+} was carried by the ethylenediaminetetraacetic acid (EDTA) titration method, and the details are as follows: the sucked sample was placed in a conical flask, in which 2 M hydrochloric acid (HCl) solution was used to adjust the pH of the sample to 5−6, and then 2 mL of an acetic acid−sodium acetate buffer solution was added with two drops of 0.2 wt % xylenol orange as an indicator. A 0.10 M EDTA standard solution was employed for complexometric titration.

3. RESULTS AND DISCUSSION

3.1. Dendrite-Free ZSB Driven by the Ion Motor. In order to facilitate the observation of the electrolyte flow effect by the ion motor, a dendrite-free ZSB was assembled for demonstration. The schematic illustration of the battery

https://doi.org/10.1021/acsami.2c06146
ACS Appl. Mater. Interfaces 2022, 14, 30839−30846

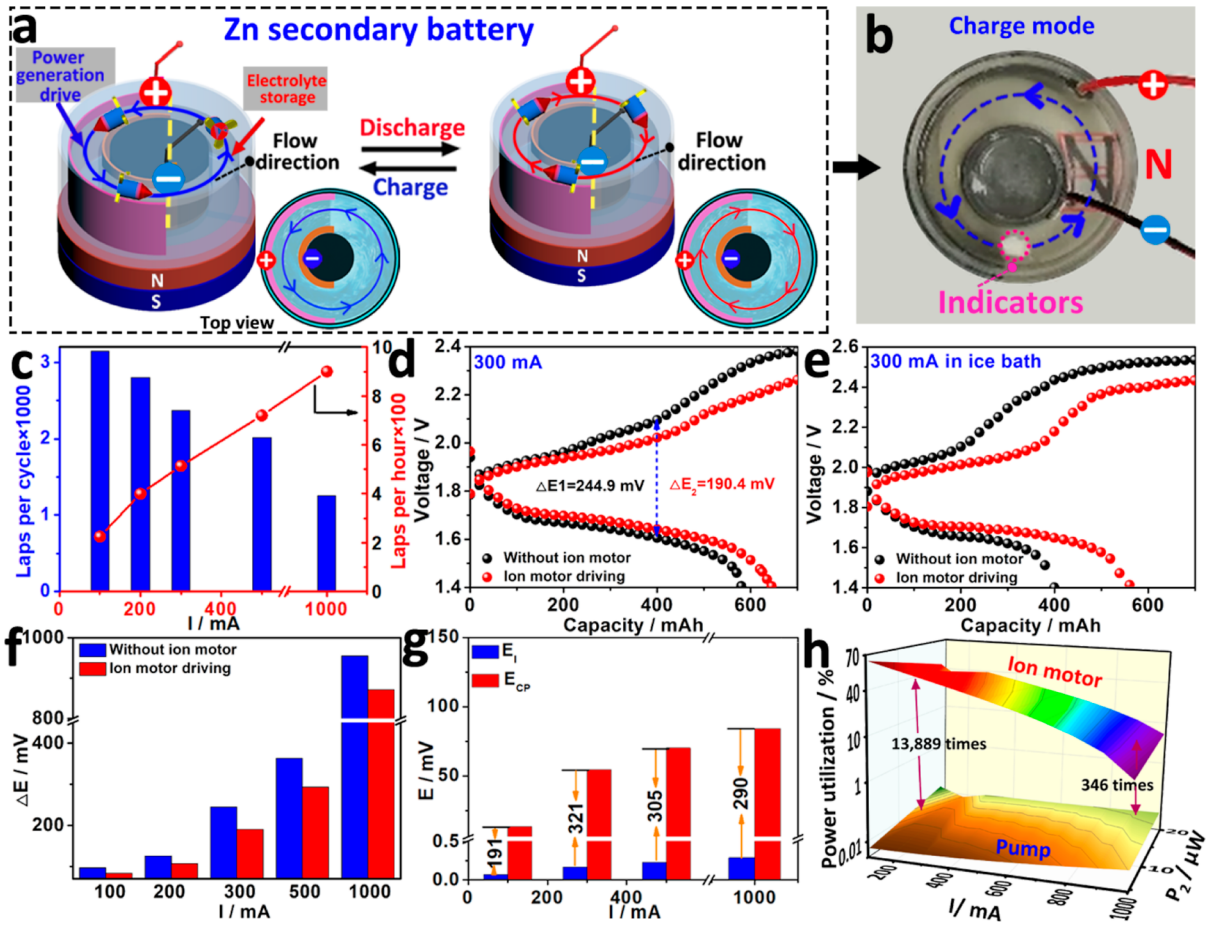

Figure 2. Electrochemical properties of the ion motor-driven ZSB. (a) Ion motor-driven ZSB. (b) Picture of the lab-scale ion motor-driven ZSB. (c) Number of laps of electrolyte circling at different currents. (d) Voltage profiles of the ZSB at 300 mA with/without ion motor driving. (e) Voltage profiles of the ZSB at 300 mA with ion motor driving (red curve) and without ion motor driving (black curve). (f) E_{CP} value generated with/without ion motor driving at different currents. (g) Profiles of E_I values and the elimination of E_{CP} by the ion motor and the additional benefit generated by the ion motor. (h) 3D profiles of power utilization of the ion motor and pump-driven electrolyte flow under different currents.

structure is shown in Figures 2a and S1, in which the magnet is placed underneath the cell with the N pole upward and S pole downward. Movie S1 shows the operation process of the battery during the charging process: When the battery is charged at 100 mA, current flows from the positive electrode to the negative electrode and the cations which constitute the current being pushed by the magnetic effect to move in the perpendicular direction, leading to the electrolyte to swirl around counter-clockwise, as shown by the floating indicator. Figure 2b is the overhead view photo of the battery during the charging process. After charging for 89 s, when the magnetic field is removed, the electrolyte flow stops with a gradual slowing move due to inertia for a short time. When the magnetic field direction is turned over with the S pole upward at the 136th second, the electrolyte starts to circle clockwise immediately, as shown in Movie S1. Besides, when the current is increased to 500 mA, it can be seen that the flow speed of the electrolyte increases obviously, as shown in Movie S2. Therefore, the flow speed and direction of electrolytes driven by the ion motor are dependent on the strength and direction of both the ion current and the magnetic field. Figures 2c, S2, and Table S1 show that with increasing current, the electrolyte swirling speed (laps per hour) increases, but the laps per cycle of charge−discharge reduce because the time spent per cycle considerably decreases. Besides, the low Reynolds number (*Re*) limit results in kinematic reversibility, which facilitates the laminar flow of liquids within narrow confinements. Figure 2d indicates the overpotential (190.4 mV) of the ZSB with an ion motor is much lower than that (244.9 mV) of ZSB without the ion motor at 300 mA, demonstrating that electrolyte flow effectively eliminates the concentration polarization caused by the gravity field. In addition, the battery undergoes poor electrolyte diffusion and low effective capacity in winter. We find that the ion motor greatly improves the output performance of the battery at low temperatures by eliminating the concentration polarization of the electrolyte. Figure 2e shows the comparison of the low-temperature performance of batteries with and without ionic motor driving. Without the ion motor, the ZSB only provides a discharge capacity of 410 mAh at −18 °C at 300 mA, maintaining only 63.6% of that at room temperature. In comparison, the ZSB driven by the ion motor provides 554 mA h, 35% higher than the ZSB without the ion motor and still maintains 86% at room temperature. This performance is very beneficial for improving future vehicles, reducing the performance degradation at low temperatures in winter. Figures 2f, S3, and S4 show the ZSB with the ion motor at different currents has lower concentration polarization and higher energy efficiency than the ZSB without the ion motor, following the effect of electrolyte flow on the three-electrode system (Figures S5−

https://doi.org/10.1021/acsami.2c06146
ACS Appl. Mater. Interfaces 2022, 14, 30839−30846

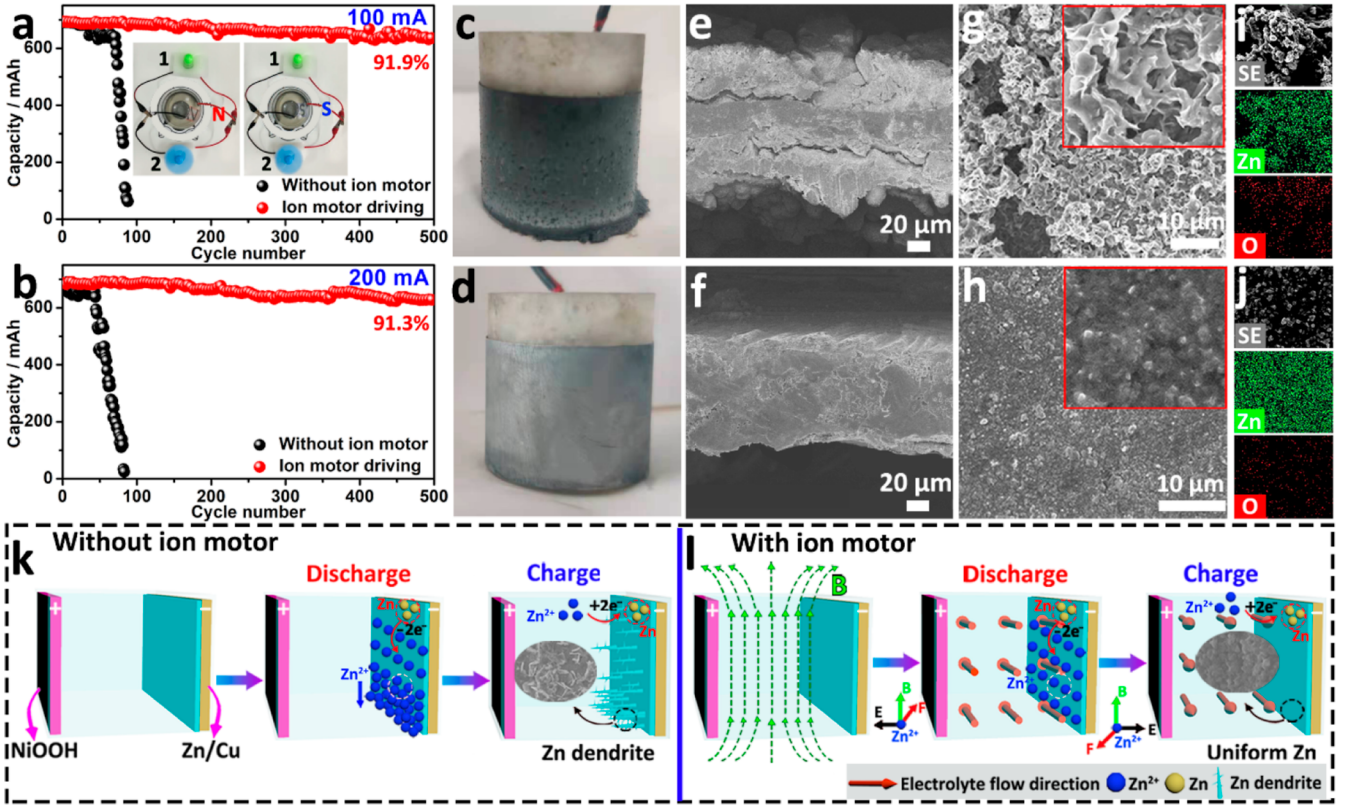

Figure 3. Cycling tests of ZSBs with/without ion motor driving at current densities of (a) 100 and (b) 200 mA. The insets in (a) are photographs of two fans powered by the ion motor-driven ZSB. Photos of the Zn electrode without (c) and with ion motor driving (d). Cross-sectional image of SEM, front-face SEM images, and corresponding elemental mapping images of the Zn electrode (e,g,i) without ion motor driving and (f,h,j) with ion motor driving after 500 cycles, respectively. The schematic illustration shows the metallic Zn deposition/stripping processes without (k) and with ion motor driving (l).

S7). Figure 2g and Table S2 further analyze the relationship between the induced electromotive force ($E_I = BLv$) and the reduction of concentration polarization (E_{CP}) affected by the ion motor. It can be found that the induced tiny E_I can eliminate a considerable E_{CP}, achieving an effect of hundred times, which significantly improves the output power and energy efficiency of the battery. In order to figure out whether the induced electromotive force of the ion motor can meet the power requirement for driving the electrolyte, a calculation was carried out according to the formula $P_2 = mv^2/2t$. Results demonstrate that the minimum power required for driving 100 mL of the electrolyte (P_2) is 4.7−18.9 μW in the current range of 100−1000 mA, which is less than the power of the ion motor (P_1, 7.2−289 μW), suggesting that the ion motor is quite competent to drive the electrolyte, particularly at higher current. Generally, a mechanical pump employed in laboratories has the least power of 0.1 W estimated based on experience. Therefore, the power of the actual mechanical pump is much higher than that of the ion motor, showing that the power efficiency of traditional mechanical pumps is less than 1% (4.7×10^{-3} to 1.89×10^{-2}%) relative to ion motor driving (Figure 2h and Tables S3 and S4). Surprisingly, the power utilization by the ion motor to drive the electrolyte reaches 65.3% (=4.7 × 100%/7.2) to 6.5% in the range of 100−1000 mA, which is 346 times to 13,889 times that of the pump driving, showing significant saving of energy. The detailed calculation process is described in the Supporting Information.

Figure 3a,b shows the long-term cycle stability performance of the ZSB driven by the ion motor at 100 and 200 mA, respectively. Without ion motor driving, the discharge capacity of the ZSB at 100 mA decays sharply and the battery fails to work after 73 cycles (black curve in Figure 3a). The red curve in Figure 3a shows that the ZSB is driven by the ion motor still has a capacity retention rate of 91.9% after 500 cycles. Particularly, at a higher current of 200 mA, the ZSB without ion motor driving fails to work after 45 cycles (Figure 3b), while the ion motor-driven battery has a discharge capacity retention higher than 91.3% throughout the 500 cycles, showing a negligible decay and demonstrating excellent electrochemical performance. Movie S3 shows the ion motor-driven ZSB drives two electric fans to rotate at high speed (the insets in Figure 3a) during 500 cycles, indicating superb stability and practical usage ability. Furthermore, we investigated the dendrite growth of Zn electrodes with and without ion motor driving (Figure 3c,d). The cross-sectional SEM images show that a rough surface is formed on the surface of Zn metal without ion motor driving (Figure 3e), while the surface structure of Zn metal with ion motor is relatively planar and dense without obvious cracks (Figure 3f). The front-face images of SEM indicate that a large number of zinc dendrites are generated on the surface of the zinc electrode without the ion motor in Figure 3g, which can cause short circuits and failure of the battery. Figure 3h reveals that the surface of the zinc electrode remains flat and smooth after 500 cycles due to the elimination of concentration polarization by the ion motor. Besides, the presence of Zn and O elements in the EDS

https://doi.org/10.1021/acsami.2c06146
ACS Appl. Mater. Interfaces 2022, 14, 30839−30846

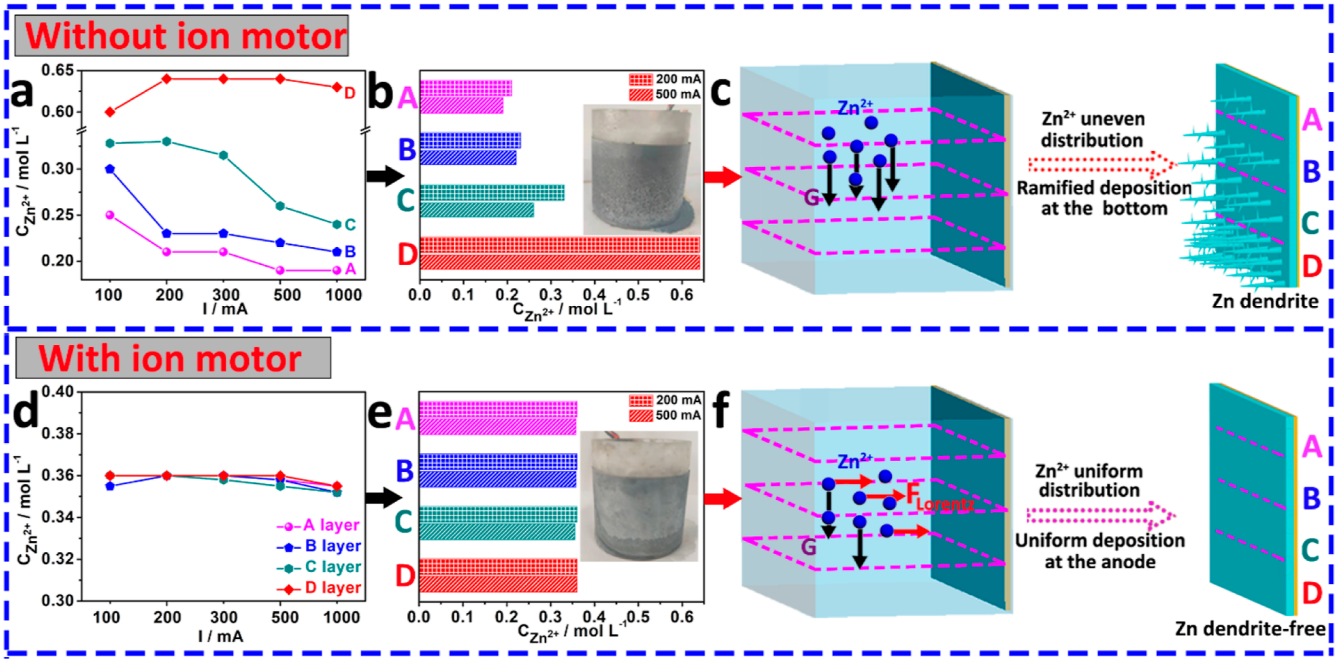

Figure 4. Distribution of Zn^{2+} ion concentration (a) without and (d) with ion motor driving in different areas under different currents (100−1000 mA). Distribution of Zn^{2+} ion concentration in an electrolyte (b) without and (e) with ion motor driving under currents of 200 and 500 mA. The schematic illustration of suppressing Zn dendrites without (c) and with (f) ion motor during the charging−discharging process via promoting Zn^{2+} ion distribution on the anode.

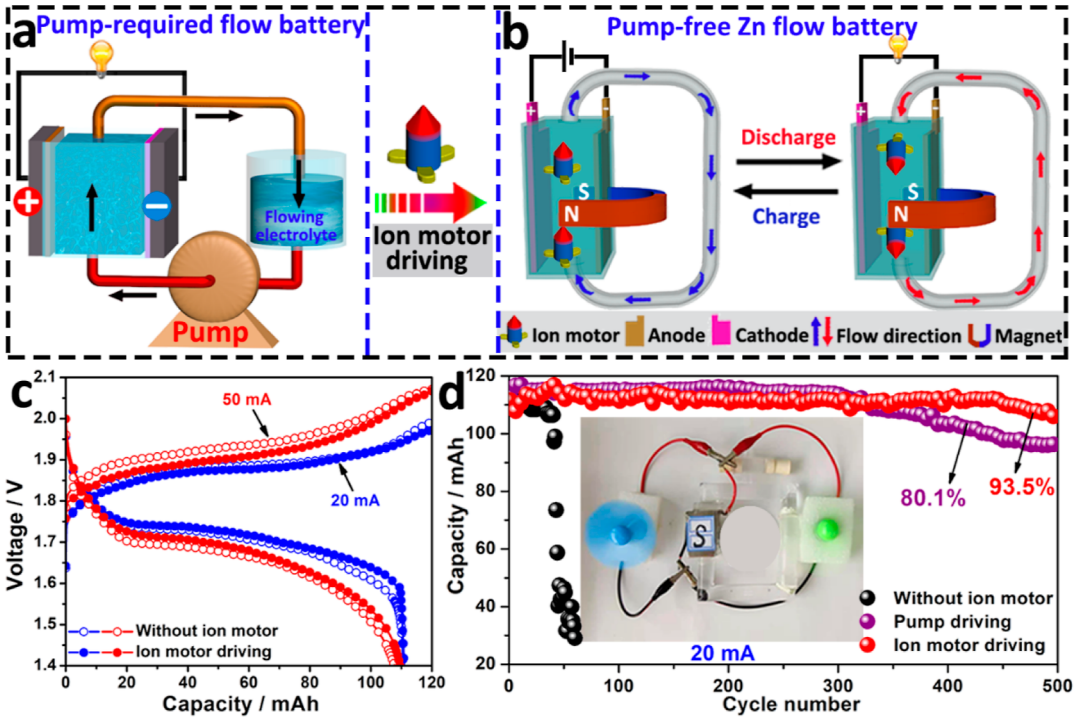

Figure 5. Electrochemical properties of ion motor-driven pump-free ZFB prototype. The models of the (a) traditional flow battery driven by the pump, (b) ion motor-driven pump-free ZFB. (c) Voltage profiles of ZFB at various currents of 20 and 50 mA with/without ion motor driving. (d) Cycling test of the ZFBs with/without ion motor driving and pump driving ZFB at a current of 20 mA; inset in (d) shows the photograph of two fans powered by the pump-free ZFB.

analysis proves that the loose zinc dendrites with a high specific surface are easily oxidized into ZnO in air without ion motor driving (Figures 3i and S8). In contrast, the dense electrodeposited zinc obtained with ion motor driving is not easy to oxidize (Figures 3j and S9). Generally, the zinc ions sinking at the lower part of the electrode of the ZSB during the discharge process will preferentially become the growth nucleus of zinc deposition for the next charging process, thus accelerating the growth of zinc dendrites and causing the failure of ZSBs.[33−39] In comparison, the ZSB driven by the ion motor eliminates the

https://doi.org/10.1021/acsami.2c06146
ACS Appl. Mater. Interfaces 2022, 14, 30839−30846

concentration gradient of zinc ions due to the continuous and stable flowing, thereby effectively inhibiting the growth of zinc dendrites (Figure 3k,l).[40−42] We used a microsyringe to further analyze zinc ion concentration in the four areas along the zinc anode surface, which is described in detail in the Supporting Information. Figures 4a−b reveals that for the ZSB without the ion motor, the zinc ion concentration in the top area (A) decreases from the initial 0.35 M to below 0.2 M after six cycles. However, the zinc ion concentration in the bottom area (D) increases to its saturation concentration (0.65 M) at currents higher than 200 mA. Figures 4d,e and S10 show that the concentrations of zinc ions in all four areas almost remain stable, about 0.35−0.36 M in the ion motor-driven mode. The uniform Zn^{2+} ion distribution effectively guarantees the uniformity of the zinc electrodeposition process (Figure 4c,f).

3.2. Pump-Free ZFB Driven by the Ion Motor. Generally, the existing flow battery is equipped with 1−2 pumps[43] (Figure 5a). Figures 5b and S11−S14 show the structure of a pump-free ZFB designed in accordance with the ion motor strategy. Figures 5c, S15, and S16 show that ZFB with ion motor driving at 10−70 mA demonstrates a higher working voltage and longer time than the battery without the ion motor. As shown in Figure 5d, the ZFB with the pump driving maintains a satisfactory capacity retention rate (80.1%) during the 500 cycles. It is worth noting that the ZFB with the ion motor shows a much higher capacity retention rate of 93.5% during the same cycles. The reason for such a significant difference is that the mechanical pump only drives the electrolyte overall in a macroscopic view, but on the microscopic observation, in the bulk solution, the move is not uniform, meaning that the concentration polarization is not relieved in some parts but not in every part with certain dead angles. In contrast, the ion motor drives electrolyte moving uniformly because the ion motor is constructed by ion flow and ion flows from one electrode to the opposite electrode, demonstrating "where there is ion flow, there is ion motor", meaning that the relieving of concentration polarization is all over without dead spaces. Unfortunately, the ZFB without the ion motor fails to work after 50 cycles due to severe zinc dendrite formation. The above results confirm that the ion motor can well replace the mechanical pump to successfully drive electrolyte movement and inhibit the growth of zinc dendrites, thereby prolonging the service life of the battery. The inset of Figure 5d shows the two fans are powered by the ZFB, and Movie S4 shows they rotate during the discharge, demonstrating the actual application ability of the ion motor-driven battery.

4. CONCLUSIONS

In summary, we report a new concept of ion motors for the durable, stable, and self-adaptive electrolyte flow in batteries. It has two prototype applications in a dendrite-free ZSB and a pump-free ZFB. The study shows that this strategy successfully eliminates the concentration gradient caused by the gravitational field via a permanent magnetic field, which suppresses the concentration polarization and dendrite growth generated during the charging and discharging process, thereby significantly improving the output performance and energy efficiency of the battery. It has the following three advantages:

(1) In the application of the dendrite-free ZSB driven by the ion motor, the tiny induced counter electromotive force generated by the ion motor can eliminate a considerable concentration polarization, achieving an efficiency of hundreds of times.

(2) The drive efficiency of the ion motor is hundreds of times that of a mechanical pump, and the cycle life of the ion motor-driven battery is much longer than that of ordinary batteries.

(3) In the application of the pump-free ZFB, the ion motor strategy not only greatly simplifies the structure of the flow battery and reduces the battery manufacture and maintenance cost but also significantly improves cycle stability and energy efficiency.

The ion motor strategy is expected to be a universal and efficient measure for improving the low-temperature performance of secondary batteries such as lithium-ion batteries, eliminating dendrites from metal secondary batteries, and developing more pump-free flow batteries and reducing water-splitting voltage.

■ ASSOCIATED CONTENT

Supporting Information

The Supporting Information is available free of charge at https://pubs.acs.org/doi/10.1021/acsami.2c06146.

Electrochemical properties of the electrodes in a three-electrode system, CV curves, linear sweep voltammetry curves, GCD profiles, EDS spectrum, and pictures of the ZSB device and pump-free ZFB (PDF)

Description of the movies (PDF)

Rotation direction and speed of the electrolyte of the ZSB in the ion motor-driven mode at a current of 100 mA (MP4)

Rotation direction and speed of the electrolyte of the ZSB in the ion motor-driven mode at a current of 500 mA (MP4)

Two fans powered by the ZSB in the ion motor-driven mode (MP4)

Fan powered by the pump-free ZFB with and without the ion motor-driven mode (MP4)

■ AUTHOR INFORMATION

Corresponding Authors

Junqing Pan − *State Key Laboratory of Chemical Resource Engineering, College of Chemistry, Beijing University of Chemical Technology, Beijing 100029, China;* orcid.org/0000-0002-7845-6468; Email: jqpan@buct.edu.cn

Xifei Li − *Xi'an Key Laboratory of New Energy Materials and Devices, Institute of Advanced Electrochemical Energy & School of Materials Science and Engineering, Xi'an University of Technology, Xi'an 710048, China;* orcid.org/0000-0002-4828-4183; Email: xfli2011@hotmail.com

Xueliang Sun − *Department of Mechanical and Materials Engineering, University of Western Ontario, London, Ontario N6A 5 B9, Canada;* orcid.org/0000-0003-0374-1245; Email: xsun9@uwo.ca

Authors

Lulu Chai − *State Key Laboratory of Chemical Resource Engineering, College of Chemistry, Beijing University of Chemical Technology, Beijing 100029, China*

Xiaoyang Zhu − *State Key Laboratory of Chemical Resource Engineering, College of Chemistry, Beijing University of Chemical Technology, Beijing 100029, China*

https://doi.org/10.1021/acsami.2c06146
ACS Appl. Mater. Interfaces 2022, 14, 30839−30846

Yanzhi Sun − *State Key Laboratory of Chemical Resource Engineering, College of Chemistry, Beijing University of Chemical Technology, Beijing 100029, China;* orcid.org/0000-0002-3871-4047

Xiaoguang Liu − *State Key Laboratory of Chemical Resource Engineering, College of Chemistry, Beijing University of Chemical Technology, Beijing 100029, China*

Wei Li − *Department of Engineering Technology and Texas Center for Superconductivity, University of Houston, Houston, Texas 77204, United States*

Jinjie Qian − *Key Laboratory of Carbon Materials of Zhejiang Province, College of Chemistry and Materials Engineering, Wenzhou University, Wenzhou 325000, China;* orcid.org/0000-0002-9996-7929

Complete contact information is available at: https://pubs.acs.org/10.1021/acsami.2c06146

Author Contributions

L.C. and J.P. conceived and designed the overall research. L.C. executed the experiment plans, material characterizations, electrochemical measurements and wrote the manuscript; X.Z. and Y.S. contributed to the discussion of the experimental design and results; X.L., W.L., J.Q., X.L., and X.S. revised the manuscript; J.P. proposed the whole concept, edited the article, and provide project funds; all authors contributed to the development of the manuscript and discussions as the project developed.

Notes

The authors declare no competing financial interest.

■ ACKNOWLEDGMENTS

This work was financially supported by the National Key Research and Development Program of China (2019YFC1908304), National Natural Science Foundation of China (21676022 and 21706004), and the Fundamental Research Funds for the Central Universities (BHYC1701A).

■ ABBREVIATIONS

EES, electrochemical energy storage
ZSB, zinc secondary battery
ZFB, Zn flow battery
Re, Reynolds number
E_I, induced electromotive force
E_{CP}, concentration polarization
SEM, scanning electron microscopy
CV, cyclic voltammetry
GCD, galvanostatic charge−discharge

■ REFERENCES

(1) Xie, J.; Lu, Y.-C. A retrospective on lithium-ion batteries. *Nat. Commun.* **2020**, *11*, 2499.
(2) Zhao, C.; Wang, Q.; Yao, Z.; Wang, J.; Sánchez-Lengeling, B.; Ding, F.; Qi, X.; Lu, Y.; Bai, X.; Li, B.; Li, H.; Aspuru-Guzik, A.; Huang, X.; Delmas, C.; Wagemaker, M.; Chen, L.; Hu, Y.-S. Rational design of layered oxide materials for sodium-ion batteries. *Science* **2020**, *370*, 708−711.
(3) Jin, C.; Liu, T.; Sheng, O.; Li, M.; Liu, T.; Yuan, Y.; Nai, J.; Ju, Z.; Zhang, W.; Liu, Y.; Wang, Y.; Lin, Z.; Lu, J.; Tao, X. Rejuvenating dead lithium supply in lithium metal anodes by iodine redox. *Nat. Energy* **2021**, *6*, 378−387.
(4) Guo, Z.; Huang, J.; Dong, X.; Xia, Y.; Yan, L.; Wang, Z.; Wang, Y. An organic/inorganic electrode-based hydronium-ion battery. *Nat. Commun.* **2020**, *11*, 959.
(5) Zhou, T.; Zhao, Y.; El Kazzi, M.; Choi, J. W.; Coskun, A. Stable Solid Electrolyte Interphase Formation Induced by Monoquat-Based Anchoring in Lithium Metal Batteries. *ACS Energy Lett.* **2021**, *6*, 1711−1718.
(6) Bayaguud, A.; Luo, X.; Fu, Y.; Zhu, C. Cationic Surfactant-Type Electrolyte Additive Enables Three-Dimensional Dendrite-Free Zinc Anode for Stable Zinc-Ion Batteries. *ACS Energy Lett.* **2020**, *5*, 3012−3020.
(7) Kopač Lautar, A.; Bitenc, J.; Rejec, T.; Dominko, R.; Filhol, J.-S.; Doublet, M.-L. Electrolyte Reactivity in the Double Layer in Mg Batteries: An Interface Potential-Dependent DFT Study. *J. Am. Chem. Soc.* **2020**, *142*, 5146−5153.
(8) Yi, Z.; Chen, G.; Hou, F.; Wang, L.; Liang, J. Strategies for the Stabilization of Zn Metal Anodes for Zn-Ion Batteries. *Adv. Energy Mater.* **2020**, *11*, 2003065.
(9) Deng, L.; Goh, K.; Yu, F.-D.; Xia, Y.; Jiang, Y.-S.; Ke, W.; Han, Y.; Que, L.-F.; Zhou, J.; Wang, Z.-B. Self-optimizing weak solvation effects achieving faster low-temperature charge transfer kinetics for high-voltage $Na_3V_2(PO_4)_2F_3$ cathode. *Energy Storage Mater.* **2022**, *44*, 82−92.
(10) Tian, Y.; An, Y.; Wei, C.; Xi, B.; Xiong, S.; Feng, J.; Qian, Y. Recent Advances and Perspectives of Zn-Metal Free "Rocking-Chair"-Type Zn-Ion Batteries. *Adv. Energy Mater.* **2021**, *11*, 2002529.
(11) Chen, X.; Hopkins, B. J.; Helal, A.; Fan, F. Y.; Smith, K. C.; Li, Z.; Slocum, A. H.; McKinley, G. H.; Carter, W. C.; Chiang, Y.-M. A low-dissipation, pumpless, gravity-induced flow battery. *Energy Environ. Sci.* **2016**, *9*, 1760−1770.
(12) Zhao, E. W.; Liu, T.; Jónsson, E.; Lee, J.; Temprano, I.; Jethwa, R. B.; Wang, A.; Smith, H.; Carretero-González, J.; Song, Q.; Grey, C. P. In situ NMR metrology reveals reaction mechanisms in redox flow batteries. *Nature* **2020**, *579*, 224−228.
(13) Yao, Y.; Lei, J.; Shi, Y.; Ai, F.; Lu, Y.-C. Assessment methods and performance metrics for redox flow batteries. *Nat. Energy* **2021**, *6*, 582−588.
(14) De La Peña, L.; Guo, R.; Cao, X.; Ni, X.; Zhang, W. Accelerating the energy transition to achieve carbon neutrality. *Resour., Conserv. Recycl.* **2022**, *177*, 105957.
(15) Ahmadiparidari, A.; Warburton, R. E.; Majidi, L.; Asadi, M.; Chamaani, A.; Jokisaari, J. R.; Rastegar, S.; Hemmat, Z.; Sayahpour, B.; Assary, R. S.; Narayanan, B.; Abbasi, P.; Redfern, P. C.; Ngo, A.; Vörös, M.; Greeley, J.; Klie, R.; Curtiss, L. A.; Salehi-Khojin, A. A Long-Cycle-Life Lithium-CO_2 Battery with Carbon Neutrality. *Adv. Mater.* **2019**, *31*, 1902518.
(16) Wu, F.; Argyle, M. D.; Dellenback, P. A.; Fan, M. Progress in O_2 separation for oxy-fuel combustion-A promising way for cost-effective CO_2 capture: A review. *Prog. Energy Combust. Sci.* **2018**, *67*, 188−205.
(17) Wang, K.; Liu, X.; Pei, P.; Xiao, Y.; Wang, Y. Guiding bubble motion of rechargeable zinc-air battery with electromagnetic force. *Chem. Eng. J.* **2018**, *352*, 182−187.
(18) Wang, K.; Pei, P.; Pei, Y.; Ma, Z.; Xu, H.; Chen, D. Magnetic field induced motion behavior of gas bubbles in liquid. *Sci. Rep.* **2016**, *6*, 21068.
(19) Wang, K.; Pei, P.; Zuo, Y.; Wei, M.; Wang, H.; Zhang, P.; Chen, Z.; Shang, N. Magnetic zinc-air batteries for storing wind and solar energy. *iScience* **2022**, *25*, 103837.
(20) Wang, K.; Liao, C.; Wang, W.; Xiao, Y.; Liu, X.; Zuo, Y. Removal of Gas Bubbles on an Electrode Using a Magnet. *ACS Appl. Energy Mater.* **2020**, *3*, 6752−6757.
(21) Han, X.; Li, X.; White, J.; Zhong, C.; Deng, Y.; Hu, W.; Ma, T. Metal-Air Batteries: From Static to Flow System. *Adv. Energy Mater.* **2018**, *8*, 1801396.
(22) Huang, A.; Liu, H.; Manor, O.; Liu, P.; Friend, J. Enabling Rapid Charging Lithium Metal Batteries via Surface Acoustic Wave-Driven Electrolyte Flow. *Adv. Mater.* **2020**, *32*, 1907516.
(23) Ko, S.-T.; Park, S.-S.; Lee, J.-H. Regenerative Battery Charging Control Method for PMSM Drive without a DC/DC Converter. *Electronics* **2019**, *8*, 1126.

(24) Pugach, M.; Parsegov, S.; Gryazina, E.; Bischi, A. Output feedback control of electrolyte flow rate for Vanadium Redox Flow Batteries. *J. Power Sources* **2020**, *455*, 227916.
(25) Li, J.; Lin, Q.; Zheng, Z.; Cao, L.; Lv, W.; Chen, Y. How Is Cycle Life of Three-Dimensional Zinc Metal Anodes with Carbon Fiber Backbones Affected by Depth of Discharge and Current Density in Zinc-Ion Batteries? *ACS Appl. Mater. Interfaces* **2022**, *14*, 12323−12330.
(26) Feng, X.; Ren, D.; He, X.; Ouyang, M. Mitigating Thermal Runaway of Lithium-Ion Batteries. *Joule* **2020**, *4*, 743−770.
(27) Chen, Y.; Dou, X.; Wang, K.; Han, Y. Lithium Dendrites Inhibition via Diffusion Enhancement. *Adv. Energy Mater.* **2019**, *9*, 1900019.
(28) Xiao, J. How lithium dendrites form in liquid batteries. *Science* **2019**, *366*, 426−427.
(29) Li, X.; Gao, P.; Lai, Y.-Y.; Bazak, J. D.; Hollas, A.; Lin, H.-Y.; Murugesan, V.; Zhang, S.; Cheng, C.-F.; Tung, W.-Y.; Lai, Y.-T.; Feng, R.; Wang, J.; Wang, C.-L.; Wang, W.; Zhu, Y. Symmetry-breaking design of an organic iron complex catholyte for a long cyclability aqueous organic redox flow battery. *Nat. Energy* **2021**, *6*, 873−881.
(30) Sun, W.; Wang, F.; Zhang, B.; Zhang, M.; Küpers, V.; Ji, X.; Theile, C.; Bieker, P.; Xu, K.; Wang, C.; Winter, M. A rechargeable zinc-air battery based on zinc peroxide chemistry. *Science* **2021**, *371*, 46−51.
(31) Noack, J.; Roznyatovskaya, N.; Herr, T.; Fischer, P. The Chemistry of Redox-Flow Batteries. *Angew. Chem., Int. Ed.* **2015**, *54*, 9776−9809.
(32) Esan, O. C.; Shi, X.; Pan, Z.; Huo, X.; An, L.; Zhao, T. S. Modeling and Simulation of Flow Batteries. *Adv. Energy Mater.* **2020**, *10*, 2000758.
(33) Jia, H.; Wang, Z.; Tawiah, B.; Wang, Y.; Chan, C.-Y.; Fei, B.; Pan, F. Recent advances in zinc anodes for high-performance aqueous Zn-ion batteries. *Nano Energy* **2020**, *70*, 104523.
(34) Yang, Q.; Li, Q.; Liu, Z.; Wang, D.; Guo, Y.; Li, X.; Tang, Y.; Li, H.; Dong, B.; Zhi, C. Dendrites in Zn-Based Batteries. *Adv. Mater.* **2020**, *32*, 2001854.
(35) Hu, E.; Yang, X.-Q. Rejuvenating zinc batteries. *Nat. Mater.* **2018**, *17*, 480−481.
(36) Hagopian, A.; Doublet, M.-L.; Filhol, J.-S. Thermodynamic origin of dendrite growth in metal anode batteries. *Energy Environ. Sci.* **2020**, *13*, 5186−5197.
(37) An, Y.; Tian, Y.; Xiong, S.; Feng, J.; Qian, Y. Scalable and Controllable Synthesis of Interface-Engineered Nanoporous Host for Dendrite-Free and High Rate Zinc Metal Batteries. *ACS Nano* **2021**, *15*, 11828−11842.
(38) Shen, Y.; Xu, L.; Wang, Q.; Zhao, Z.; Dong, Z.; Liu, J.; Zhong, C.; Hu, W. Root Reason for the Failure of a Practical Zn-Ni Battery: Shape Changing Caused by Uneven Current Distribution and Zn Dissolution. *ACS Appl. Mater. Interfaces* **2021**, *13*, 51141−51150.
(39) An, Y.; Tian, Y.; Zhang, K.; Liu, Y.; Liu, C.; Xiong, S.; Feng, J.; Qian, Y. Stable Aqueous Anode-Free Zinc Batteries Enabled by Interfacial Engineering. *Adv. Funct. Mater.* **2021**, *31*, 2101886.
(40) Zheng, J.; Archer, L. A. Controlling electrochemical growth of metallic zinc electrodes: Toward affordable rechargeable energy storage systems. *Sci. Adv.* **2021**, *7*, No. eabe0219.
(41) Hao, J.; Yuan, L.; Ye, C.; Chao, D.; Davey, K.; Guo, Z.; Qiao, S. Boosting Zinc Electrode Reversibility in Aqueous Electrolytes by Using Low-Cost Antisolvents. *Angew. Chem., Int. Ed.* **2021**, *60*, 7366−7375.
(42) Chen, X. R.; Zhao, B. C.; Yan, C.; Zhang, Q. Review on Li Deposition in Working Batteries: From Nucleation to Early Growth. *Adv. Mater.* **2021**, *33*, 2004128.
(43) Cheng, J.; Zhang, L.; Yang, Y.-S.; Wen, Y.-H.; Cao, G.-P.; Wang, X.-D. Preliminary study of single flow zinc-nickel battery. *Electrochem. Commun.* **2007**, *9*, 2639−2642.

https://doi.org/10.1021/acsami.2c06146
ACS Appl. Mater. Interfaces 2022, 14, 30839−30846